Rheol Acta (2008) 47:895–908
DOI 10.1007/s00397-008-0278-z

ORIGINAL CONTRIBUTION

Rheo-optic flow-induced crystallisation of polypropylene and polyethylene within confined entry–exit flow geometries

Lino Scelsi · Malcolm R. Mackley

Received: 2 November 2007 / Revised: 8 February 2008 / Accepted: 10 March 2008 / Published online: 22 April 2008
© Springer-Verlag 2008

Abstract This paper reports experimental observations on the way polypropylene (PP) and high-density polyethylene (HDPE) can crystallise during flow. Both a deep and a shallow slit geometry were chosen for the rheo-optical study. Preliminary linear viscoelastic rheological tests enabled the temperature window for quiescent crystallisation to be established. Flow-induced crystallisation (FIC) studies were performed in a temperature regime above the normal quiescent crystallisation conditions. In the case of HDPE, FIC occurred during flow at the sidewalls of the slit and in localised regions downstream and the processing pressure increased during the piston movement. In the case of PP, flow-induced crystallisation was generally observed after flow cessation, and the processing pressure did not change during flow. For PP, FIC also occurred preferentially at the walls in the form of elongated crystallites, but the fibres gradually emerged after flow cessation. The difference in the FIC behaviour was attributed to differences in both the rheology and the crystal growth kinetics of the two materials at the particular super-cooling used.

Keywords Flow-induced crystallisation · Multi-pass rheometer · Fibrous crystals

Nomenclature

FIC	flow-induced crystallisation
MPR	multi-pass rheometer
Mw	weight average molecular weight (g/mol)
Mn	number average molecular weight (g/mol)
T_C	crystallisation temperature (°C)
T_M^{DSC}	melting temperature (°C)
ΔT_{exp}	degree of super-cooling in the FIC experiments (°C)
$\dot{\gamma}_{app,w}$	apparent wall shear rate (s^{-1})
$\overline{\lambda}$	viscosity average relaxation time

L. Scelsi · M. R. Mackley (✉)
Department of Chemical Engineering, University of Cambridge,
Pembroke Street,
Cambridge CB2 3RA, UK
e-mail: mrm5@cheng.cam.ac.uk

Introduction

Flow-induced crystallisation (FIC) of polymer melts can occur in several ways. In industrial processes, different types of FIC can occur simultaneously under complex thermo-mechanical histories. In the case of injection moulding, for instance, both the complex flow and the presence of temperature gradients are responsible for the onset of different crystal morphologies that are generated in various parts of the mould. Generally, a fine trans-crystalline morphology is observed near the walls, dominated by the nucleating effect of the surface (see for example Billon et al. 2002). Further into the melt, an oriented layer is present, where crystallisation is governed by the orientation and stretch of the polymer molecules due to the flow (Jerschow and H Janeschitz-Kriegl 1996). Finally, in the core of the material, where the strain rates are often the lowest, crystallisation is generally spherulitic, and develops gradually over time after injection (Swartjes 2003).

Flow in general can either enhance spherulitic isotropic crystallisation (see for example Eder et al. 1990 and Jay et al. 1999) or induce fibrous nuclei that then form shish-kebab-like crystals (see for example Keller 1968 and Saquet et al. 2000).

The physical phenomenon that drives flow-induced crystallisation is the configuration of the polymer molecules during flow (van Meerveld et al. 2004). Flow can orient/stretch the macromolecules, and the deviation from the spherical coil configuration decreases the barrier for both crystal nucleation and growth (Keller 1968). The longest molecules in the melt (i.e. the high-molecular weight fraction) tend to orient/stretch most readily during the flow and are thought to play a key role in the development of FIC (see for example Keller and Mackley 1974, Somani et al. 2000 and Kornfield et al. 2003). Once the crystallites have nucleated and grown up to a critical number and size, they modify the local flow around the growing crystal and can also influence the primary flow (Mackley 1975). Other authors discuss the possibility of small crystal nuclei formation where polymer chains 'bridge' the nuclei and where this 'physical cross-linked' network can then be stretched by the flow (Zuidema et al. 2001), resulting in fibrous crystal nucleation. Once the nuclei have formed, other chains can crystallise around the "shish" in the form of folded lamellae "kebabs".

At present, a comprehensive model that can explain all the features of the FIC of polymers for a broad range of conditions does not exist. The prediction of the flow-induced crystallisation kinetics and the local morphology starting from observation is challenging, and currently, the modelling of flow-induced crystallisation in industrial flows is limited in most cases to using the Avrami model of nucleation and growth (Avrami 1939) as a frame of reference (see for example Doufas et al. 1999, Smirnova et al. 2005 and Zuidema et al. 2001).

Previous work on flow-induced crystallisation under complex processing flows has been carried out by several groups (see for example McHugh et al. 1991, McHugh and Khomami 1990 and Peters 2003). Mc Hugh and co-workers performed optical observations of polymer melts extruded through pseudo-2D dies and observed that, for FIC occurring in a slit with parallel walls, corresponding to a simple shear flow, highly oriented crystals formed at the walls and then propagated towards the centreline. However, oriented crystallisation occurring within a converging channel originated at the centreline, where the orientation of the molecules by the extensional flow-field is maximum.

Optical and X-ray studies of flow-induced crystallisation using a multi-pass rheometer have been carried out at Cambridge in the past years. Saquet et al. (2000) reported experimental observations on the way that flowing polyethylene melts can crystallise within a processing channel geometry. Using a multi-pass rheometer, the evolution of crystallisation was followed by rheological, rheo-optic and coupled X-ray data. The formation of the crystals occurred during flow at the wall of the slit, and this was associated by the authors to a coil-stretch transition of the polymer chains (Brochard and De Gennes 1992). More recently, Hernandez de Müller (2007) performed similar experiments and proposed a simple model to predict the increase in pressure difference due to the accumulation of fibrous crystals in the slit. The work presented in this paper extends these studies by analysing in detail the FIC of both HDPE and PP using two different flow geometries. Significant differences have now been observed between the two polymers, and rather than providing a comparison based on a complete parameter space description of FIC for PP and HDPE, the objective of this work was to provide experimental data for future numerical simulations that allow the prediction of the onset of FIC under conditions close to those encountered in industrial processing. The significant differences in the way FIC occurs for these two polymers in typical processing conditions have also been highlighted, together with the effect of slit depth on optical observations.

Experimental section

Materials

The materials used were a high-density polyethylene (HDPE), DOW96003E, and an isotactic polypropylene (iPP), Atofina M2501R. The molecular weight data and the melting temperature determined by non-isothermal DSC at 20 °C/min are shown in Table 1. Both polymers are commercial grades, contain no additives and have a log-normal molecular weight distribution.

Table 1 Molecular weight, polydispersity, melting temperature, degree of super-cooling and average relaxation time of the two materials used

Label	Description	Mw (g/mol)	Mn (g/mol)	Mw/Mn	T_M^{DSC} (°C)	$\Delta T_{\exp}$ (°C)	λ (s)	Notes
96003CPE DOW	HDPE	180k	23k	7.8	133	1–5	220	
3250MR1 ATOFINA	i-PP	213k	42.5k	5	170	35–40	~1	Isotactic index, 0.97

Molecular weights determined by size exclusion chromatography (courtesy of Dow Benelux); melting temperatures obtained by DSC
ΔT_{exp} typical values of the degree of super-cooling used during the FIC experiments, $\bar{\lambda}$ viscosity average relaxation time as defined in the text

Experimental techniques

Shear rheology and quiescent crystallisation times

The determination of linear viscoelastic rheology and the timescales for quiescent crystallisation provided base experimental data from which flow-induced crystallisation experiments could be carried out. The linear viscoelastic characterisation of the materials in the molten state and the determination of the quiescent crystallisation times over a wide range of temperatures were carried out using an ARES strain-controlled rheometer with 25-mm parallel plates. From frequency sweeps in the linear region (maximum strain 10%), the linear relaxation spectra of eight-mode Maxwell elements were determined for both materials (Mackley et al. 1994) at temperatures just above the temperature imposed in the subsequent crystallisation experiments, i.e. 140 and 142 °C for HDPE and PP, respectively. The spectra in terms of viscous contributions to the zero shear viscosity of the relaxation modes as a function of their characteristic relaxation times are presented in Fig. 1. At conditions close to those in the crystallisation experiments, both the magnitude of the viscosity and the viscosity contributions of the modes are different for the two samples. In the case of HDPE, the viscosity is considerably higher, and the major viscosity contributions arise from the long relaxation modes, whereas the modes dominating the viscosity of the PP sample are those in the middle of the range of relaxation times investigated. The higher viscosity of the long relaxations modes of the HDPE will influence the level of chain extension and, therefore, the potential to nucleate flow-induced crystals. This effect, combined with the faster crystallisation kinetics of HDPE, contributes to differences in the crystallisation behaviour during the FIC experiments. HDPE crystallised during flow at low degree of super-cooling, whereas PP crystallised gradually after flow cessation at higher degrees of super-cooling.

To characterise the timescales of quiescent crystallisation in the temperature range of interest, time sweeps in quasi-static conditions were performed at a constant strain of 1% and angular frequency of 10 rad/s. The samples were kept for 5 min well above their melting temperature to erase their molecular memory and then cooled in the rheometer from the melt (HDPE, from 180 to 140 °C; PP, from 190 to 142 °C).The cooling took about 3 min. Subsequently, the temperature was kept constant. The onset of crystallisation was identified from the upturn in the G′ (storage modulus) curves, as shown in Fig. 2. All the subsequent flow-induced crystallisation experiments on the two materials have been carried out at temperatures where quiescent crystallisation does not readily occur within the observation timescale of the flow experiment. Figure 2 shows that, for HDPE (Fig. 2a) at 127 °C, quiescent spherulitic crystallisation does not become rheologically significant until after 500 s. Subsequent multi-pass rheometer (MPR) flow-induced crystallisation experiments were carried out above this temperature. For the case of PP, a temperature of significant quiescent crystallisation was detected at 132 °C in a 500-s timescale, and a flow-induced crystallisation temperature of 134 °C was chosen to avoid as much as possible competition with spherulitic growth.

Processing experiments in a multi-pass rheometer

Controlled isothermal complex-flow experiments that resemble elements of polymer processing conditions were carried out using a MPR in its optical configuration. This technique has been previously described by several authors (see for example Collis and Mackley 2005). The MPR is a dual piston capillary-type rheometer designed for small quantities of material (~12 g of polymer) and consists of three sections. The top and bottom sections contain reservoirs for the polymer material, servo hydraulically driven pistons and pressure/temperature transducers. The midsection enables simultaneous pressure and optical

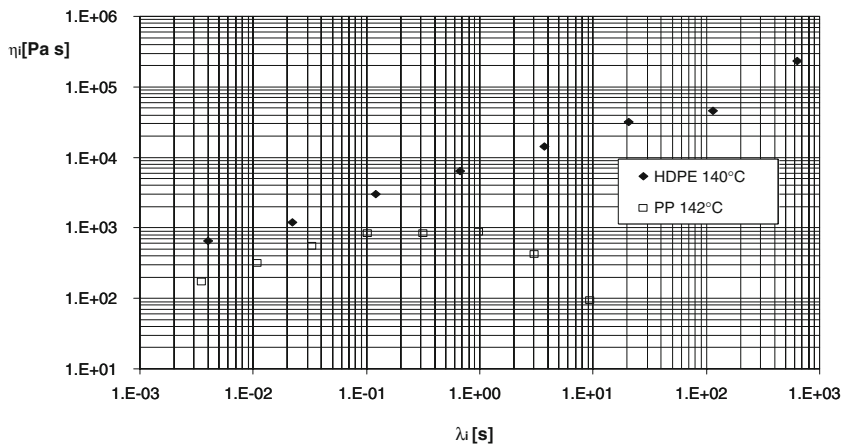

Fig. 1 Log–log plot of the viscosity η_i ($\eta_i = g_i \times \lambda_i$) associated to each mode as a function of the corresponding relaxation time λ_i, indicating the viscous component contribution for each mode, λ_i, obtained by fitting frequency sweeps of the two materials at 1% strain in an ARES rheometer with an eight-mode Maxwell model

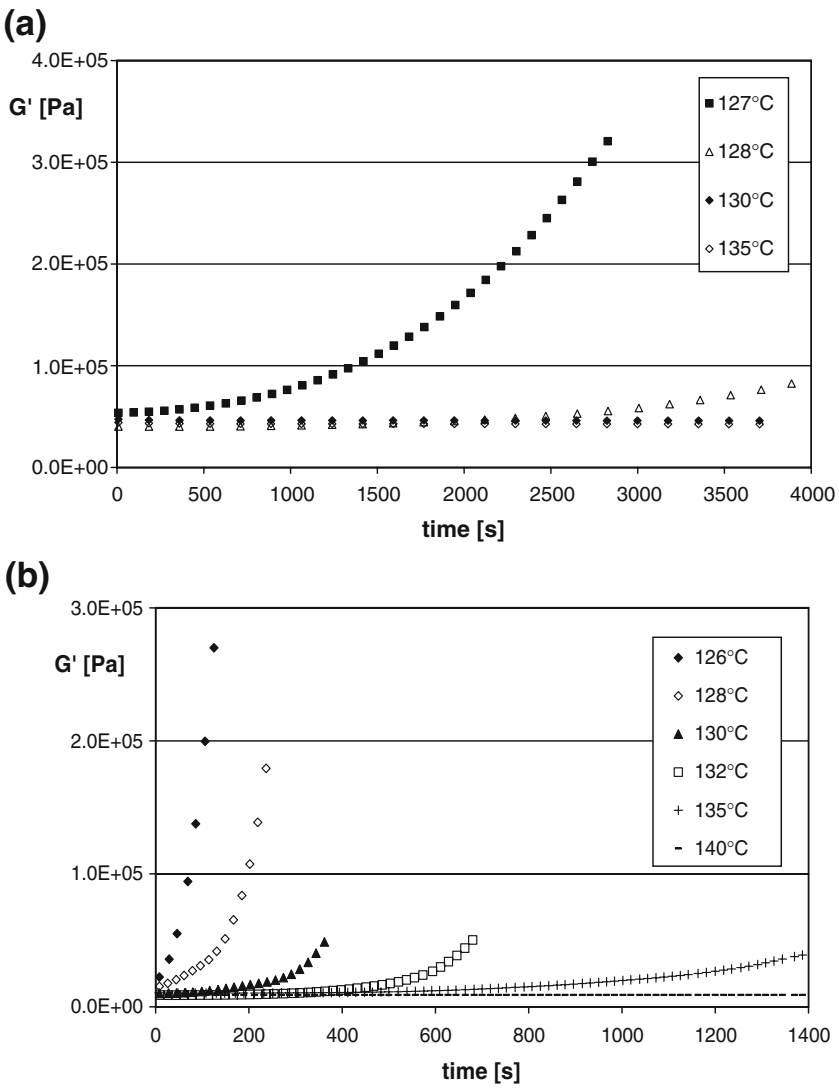

Fig. 2 Time evolution of the storage modulus of HDPE (**a**) and PP (**b**) crystallising in quasi-static conditions (strain, 1%; angular frequency, 10 rad/s) at a constant temperature (see legend) within an ARES rheometer. The upturn in the curves corresponds to the onset of crystallisation. The samples were cooled to the experimental temperature from a starting temperature of 180 °C (HDPE) or 190 °C (PP)

measurements to be made, and resembles a cube with holes through all six faces. The vertical faces accept a pair of stainless steel die inserts in one direction and a pair of stress-free quartz windows in the other while polymer flows through the top and bottom holes. All three sections are surrounded by heating channels and insulation as shown schematically in Fig. 3.

During experiments, the pistons were moved synchronously, forcing the material to flow within the contraction geometry in the midsection. Optical observation was carried out in bright field or through crossed polarisers, using monochromatic polarised light with a wavelength of 514 nm and a digital video camera. The optical train for the flow-induced birefringence (FIB) observations—polariser lens at 0°, quarterwave plate at 45°, sample between quartz windows, quarter wave plate at 135° and analyser lens at 90°—was removed for the bright-field visualisation of localised crystallisation.

Two different geometries that allow complementary observations were used, and their configuration and dimensions are shown in Fig. 4. Geometry 1 (Fig. 4a) has an optical depth 8 times greater than its width and was named “deep slit”. Being 10-mm deep and 1.25-mm wide, it has been approximated to a slit of infinite depth, in which the flow is essentially 2D, making flow-field interpretation easier (the validity of the assumption for this specific geometry has been confirmed by a study from Clemeur et al. 2004). Geometry 2 or the “shallow slit” (Fig. 4b) has a nearly square cross-section and thus is fully 3D, and the walls of the glass windows have a significant influence on flow and crystallisation. The essential advantage of the shallow slit is that it allows a higher resolution of the morphology of the polymer during flow-induced crystallisation, as in the case of PP under certain conditions, it allows visualisation of the individual spherulites.

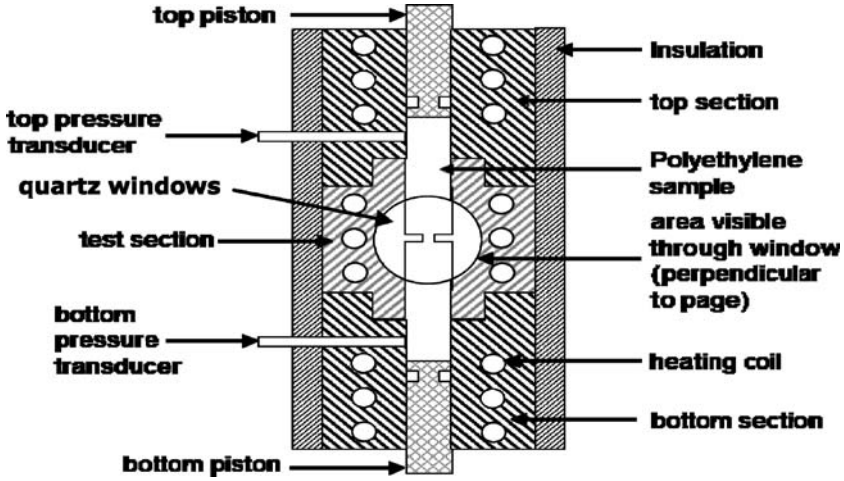

Fig. 3 Schematic view of the MPR midsection with an optical cell (courtesy of Dr. D. G. Hassell)

A mean Weissenberg number has been used as an indicator of the average rheological response of the materials and has been defined as:

$$\mathrm{We} = \dot{\gamma}_{app,w} \cdot \overline{\lambda} \tag{1}$$

where $\dot{\gamma}_{app,w}$ is the apparent wall shear rate as defined in page 8, and $\overline{\lambda}$ is a viscosity average relaxation time determined from the relaxation spectrum in the following way:

$$\overline{\lambda} = \frac{\sum_{i=1}^{N} g_i \cdot \lambda_i^2}{\sum_{i=1}^{N} g_i \cdot \lambda_i} \tag{2}$$

where g_i is the modulus and λ_i is the relaxation time of the i*th* mode. The HDPE at a reference temperature of 140 °C has a long relaxation timescale ($\overline{\lambda}$=220 s), whereas the PP at 142 °C has a much shorter relaxation time ($\overline{\lambda}$=1 s).

As the nucleation of flow-induced crystals correlates most strongly with the high-end tail of the molecular weight distribution, the Weissenberg number defined here represents merely an indication of the average relaxation timescales of the molecules in the flow but has a limited significance in modelling the onset of flow-induced crystallisation.

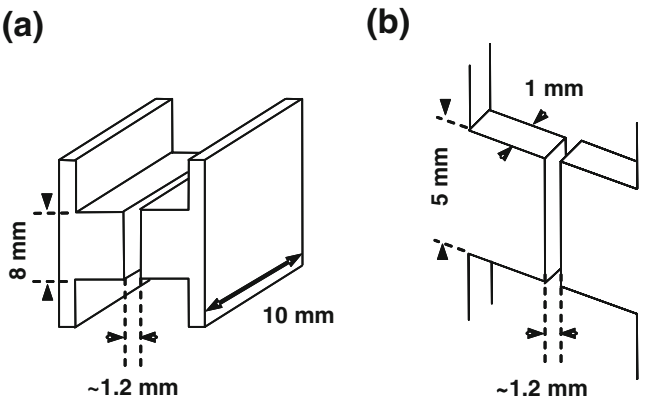

Fig. 4 **a** The deep slit (depth, 10 mm) and **b** the shallow slit (1 mm)

Melt flow birefringence

Flow-induced birefringence (FIB) observations of the melt flow were carried out close to temperatures at which crystallisation could occur. FIB is a well-established technique that allows visualisation of the principal stress difference generated by flow and hence identification of the stress distribution in the polymer (see for example Valette et al. 2006). According to a stress-optical rule, each fringe observed in the pattern represents a constant increment in the principal stress difference in the polymer fluid.

Figure 5a and b shows melt flow birefringence observations of PP and HDPE flowing downwards in the deep slit. This geometry creates regions of high simple shear near the slit walls (fringes parallel to the flow direction) and extensional flow in the region of the symmetry line in the inlet and outlet areas of the flow (fringes perpendicular to the flow direction). Due to the length of the slit (8 mm), the polymer fluid resides for a longer time in a simple shear-flow region as compared to the extensional entry and exit regions. Within the slit region, stress levels are highest at the wall and lowest at the centreline. The apparent wall shear rate used to estimate shear rates through geometry 1 was based on the solution for Newtonian flow through infinite parallel plates and is given by Eq. 3,

$$\dot{\gamma}_{app,w} = \frac{6Q}{w^2 l} = \frac{3\pi D_p^2 V_p}{2w^2 l} \tag{3}$$

where Q is the volumetric flow rate (mm^3 s^{-1}), D_p is the piston diameter (10 mm), w is the width of the slit (1.2 mm), l is the depth of the slit (10 mm) and V_p is the speed of the pistons (mm s^{-1}).

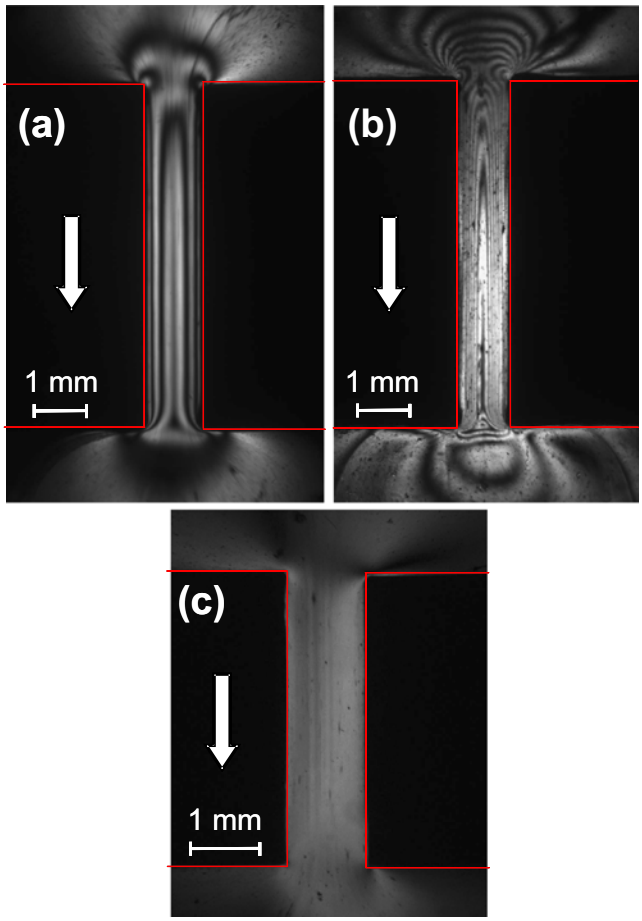

Fig. 5 Steady state FIB observation of melt flow within the midsection. **a** PP in the deep slit. T=161 °C; 5 mm/s piston speed, $\dot{\gamma}_{app,w}\approx$200 s^{-1}. **b** HDPE in the deep slit . T=140 °C; 0.5 mm/s piston speed, $\dot{\gamma}_{app,w}\approx$20 s^{-1}. The fringe pattern allows the stress distribution in the flowing polymer to be established. **c** PP in the shallow slit. T= 175 °C; 5 mm/s, $\dot{\gamma}_{app,w}\approx$2,900 s^{-1}. The shallow slit is only 1-mm deep, and, at flow conditions close to the ones in the FIC experiments, the flow birefringence fringes could not be identified

The corresponding FIB within the shallow slit contraction geometry is illustrated in Fig. 5c for PP. Because the depth of the slit is only 1 mm, the glass window walls affect the flowfield, and the stresses are more evenly distributed across the channel width. However, for the shear rates investigated, which are close to those in the FIC experiments, the stress profile cannot be identified from integer fringe counting because the birefringence levels were below that of the first extinction fringe. The hydraulic diameter of a square section corresponds to its side length, so the apparent wall shear rate used to characterise the shear rate through geometry 2 was calculated through the following approximate expression:

$$\dot{\gamma}_{app,w} = \frac{4Q}{\pi l^3} = \frac{D_p^2 V_p}{l^3} \tag{4}$$

where Q is the volumetric flow rate (mm^3 s^{-1}), D_p is the piston diameter, l is the average side length of the cross-section (1.1 mm) and V_p is the speed of the pistons (mm s^{-1}).

In geometry 2, the mechanical history that the polymer undergoes before entering the slit region is complex. The transition from 10×10 mm (square section of the midsection barrel) to 1.2×1 mm occurs in two stages, as the polymer, before entering the slit, comes in contact with a contraction generated by the presence of the windows, where the section is reduced to 10×1 mm. Due to this contraction, the crystal fibres form not only in the slit region but also upstream.

Flow-induced crystallisation

The materials and experimental conditions have been chosen to obtain the most effective visualisation of the FIC development. A birefringence image of HDPE crystallising during flow in a deep slit (Fig. 6) shows that, under the conditions described in this paper, it was not possible to simultaneously monitor the stress distribution and the flow-induced crystal formation due to an excessive number of fringes in the slit region. For this reason, subsequent crystallisation experiments were monitored only in bright field to maximise the resolution of the images. The polymer was initially held for several minutes well above the melting temperature T_M^{DSC} + 40 °C) to erase the thermo-mechanical history. Then, the oil circulator that controls the MPR temperature was set to a lower temperature value so that the sample was cooled down to the desired temperature for the crystallisation experiment. While cooling down, slow adjustments of the pistons position were needed to follow the thermal shrinkage of the sample. The pistons were then moved in single pass mode (i.e. they were moved simultaneously downwards and then stopped), and the optical observations of the crystallising polymer during and after flow were recorded by a digital camera (Q-

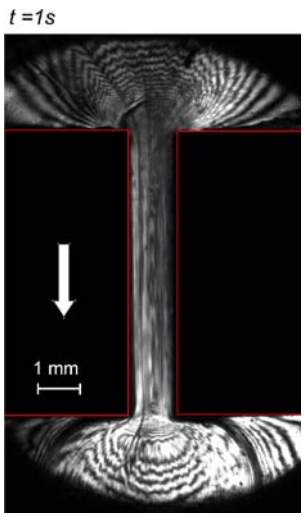

Fig. 6 Development of FIC for HDPE in the deep slit; T=130 °C; 5 mm/s, piston speed, $\dot{\gamma}_{app,w}\approx$200 s^{-1} (We=40,000). Birefringence observation of FIC occurring during flow. Image taken at t=1 s after the inception of flow. Under the conditions investigated, it was not possible to simultaneously observe the formation of flow-induced crystals and the stress distribution

imaging QI CAM FAST 1394). The pressure difference evolution was also acquired using pressure transducers (Omega Eng. PX335K-3KGV). After each experiment, the polymer was re-heated, and the pistons were gradually moved back to their original positions. In principle, it would be desirable to examine FIC of HDPE and PP at similar level of super-cooling. This however is not possible. In the experiments presented in this paper, ΔT_{PE}=1–5 °C and ΔT_{PP}=32–40 °C. Having comparably low super-coolings for PP would involve timescales of hours or days. Equally, a higher level of super-cooling for HDPE would mean that spherulitic crystallisation would occur in fractions of second. The choice of the crystallisation temperature is based on the ability to super cool the polymer and perform the FIC experiments in a realistic timeframe. These limitations are also generally reflected in industrial forming processes, where normally, in the case of HDPE, the oriented flow-induced crystals form at low super-cooling, and for PP, most of the FIC occurs at high super-cooling.

Results and discussion

HDPE DOW 96003E

Due to the low cooling rates used in the MPR (approximately 1 °C/min) and the fast crystallisation kinetics of HDPE, the experimental temperature window for FIC without spherulitic crystallisation was limited to low levels of super-cooling, 1–5 °C below the quiescent mean melting temperature determined by DSC (133 °C). Under these conditions, if the shear rate and, thus, the wall stress was above a threshold value, HDPE crystallised during flow, generating fibrous crystals.

HDPE–flow-induced crystallisation–geometry 1 (deep slit)

It was found preferable to carry out experiments using the 10-mm-depth slit for HDPE, as this gave good optical contrast and the essentially 2D flow facilitated interpretation of the results.

A series of "single pass" experiments were carried out in a temperature range in which FIC occurred. Figure 7 shows the development of flow-induced crystallisation observations within the deep slit, and Fig. 9a shows a matching pressure profile for these experiments. Figure 7 shows the time evolution of bright-field observations of FIC at 130 °C and an apparent wall shear rate of 200 s^{-1}. The very high Weissenberg number (We=44,000) is an indicator of the high level of orientation/stretch to which the polymer chains are subjected during the flow. At t=0 (Fig. 7a), flow had not yet started, and some particle debris are observable. The pistons were then moved synchronously downwards with amplitude of 10 mm. With the application of flow, fibrous crystals were formed, appearing as dark zones near the wall. Figure 7b–d shows the substantial fibrous crystal nucleation and growth from the walls of the slit, and the propagation of the crystals downstream. Figure 7d shows that, at the end of the piston movement, the flow became partly blocked by the crystals that had accumulated at the exit of the slit region. The downstream crystals were very clearly visible and formed "crystal fangs" downstream of the slit exit. Flow birefringence "fangs" without crystallisation, corresponding to regions of stress concentration at the exit of a contraction, have

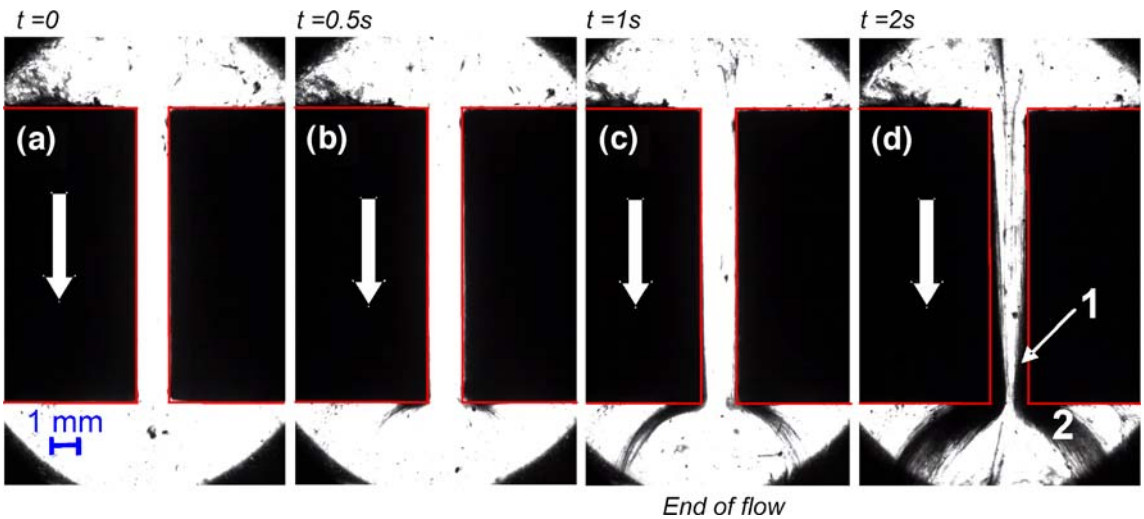

Fig. 7 Development of FIC for HDPE in the deep slit; T=130 °C; 5 mm/s piston speed, $\dot{\gamma}_{app,w}\approx$200 s^{-1} (We=40,000). Optical observation in bright field. **a** t=0 (before flow); **b**, **c** during flow; **d** t=2 s (end of flow). *1* Fibrous crystals generated at the wall, *2* downstream crystal "fangs". After the cessation of flow, the crystals formed stop evolving and are stable during the observation time (30–60 min). The flow direction is indicated by a white arrow

previously been reported by Lee et al. (2001) for LDPE flowing in a entry–exit geometry. Moreover, in a recent work using a metallocene-catalysed HDPE, Hassell and Mackley (2008) observed sharp crystal fangs forming at the outlet region of a contraction and performed a quantitative study of the growth of the crystal tip.

FIC was concentrated at the walls and in the fang regions downstream, and following flow cessation, the crystals did not significantly evolve further throughout the observation time (30–60 min), showing that, under these conditions, further FIC does not occur and the flow did not considerably enhance spherulitic crystallisation. The particle debris present at the beginning of the experiments did not appear to have a significant effect on the global flow and on crystal nucleation.

The matching pressure difference evolution for the above experiment is shown in Fig. 9a. The figure shows that the pressure difference across the midsection during the experiment at 130 °C continued to build up during the piston movement and gradually relaxed after the pistons had stopped, as opposed to a normal melt flow experiment carried out on the same material at 170 °C, where the pressure difference through the contraction quickly reached a steady state value during flow and did not change. The increase of the pressure difference during the pass at 130 °C, without attaining a steady state, was attributed to the continuous crystal formation during that time and the consequent partial slit blockage, and forms a separate study (Hernandez de Müller 2007).

HDPE–flow-induced crystallisation–geometry 2 (shallow slit)

Similar experiments were carried out for the same material using the shallow slit. The combination of observations in the two geometries allowed the differences in the flowfield to be investigated. As the depth of the shallow slit (1 mm) is similar to its width (1.2 mm), the geometry generates an essentially 3D flowfield, which is more complex to interpret but at the same time yields a higher resolution of the microstructure formation in the flowing polymer.

Figure 8 illustrates the development of flow-induced crystallisation of HDPE during a single pass within a shallow slit contraction geometry. The apparent wall shear rate (290 s^{-1}) and the temperature (130 °C) were similar to those in the previous deep slit experiments. The Weissenberg number was equal to 63,000. In addition to the occurrence of flow-induced crystallisation at the sidewalls of the slit and in the downstream "fang" region, flow-induced elongated structures formed in the central part of the field of view (Fig. 8). From a closer analysis of the moving images, it was inferred that these flow-induced fibrous crystals formed at the wall of the quartz windows. The elongated crystals were either at rest or moved slower than the bulk of the fluid, and they tended to adhere to the wall itself. The region near the glass wall represents a favourable region for crystal formation due to the higher stress and the possible nucleating effect of the surface. Figure 9b shows the matching pressure difference evolution across the midsection for the above experiment, and the data show a similar trend to those for HDPE in the deep slit where the pressure difference progressively increased during flow as FIC occurs to partially block the slit.

Key observations for FIC of HDPE are that fibrous crystallisation occurs during the pistons movement and the formation of the fibrous crystals affects the local flow conditions in which crystallisation occurs. The experiments

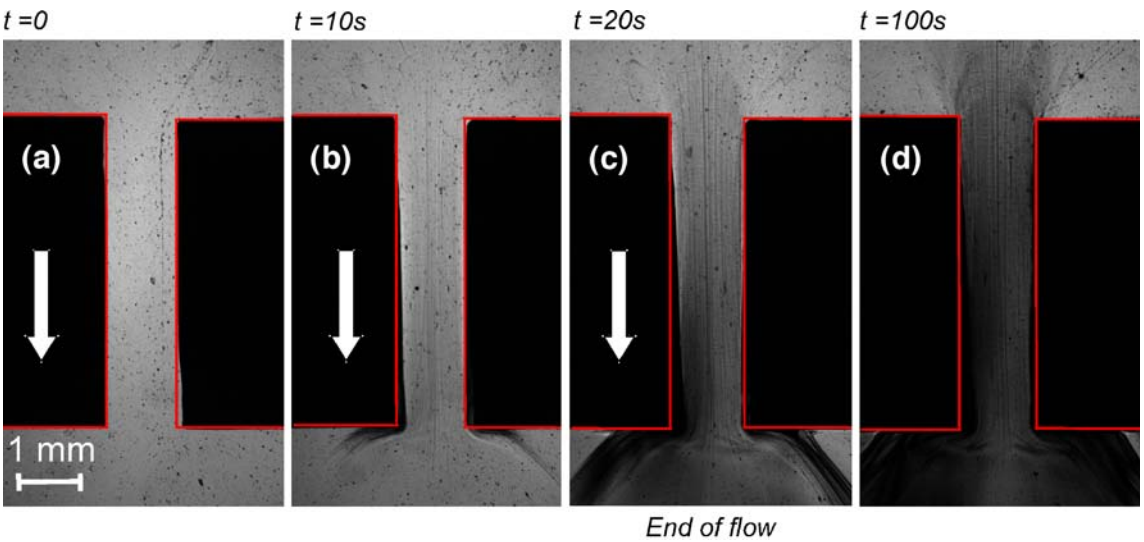

Fig. 8 Development of FIC for HDPE in the shallow slit; T=130 °C; 0.5 mm/s piston speed, $\dot{\gamma}_{app,w}\approx$290 s^{-1} (We=63,000). Optical observation in bright field. **a** t=0 (before flow), **b** during flow, **c** end of flow. After the flow cessation, further crystal development is very limited (**d**), and the crystals are stable over the observation time (approximately 30 min). The flow direction is indicated by a white arrow

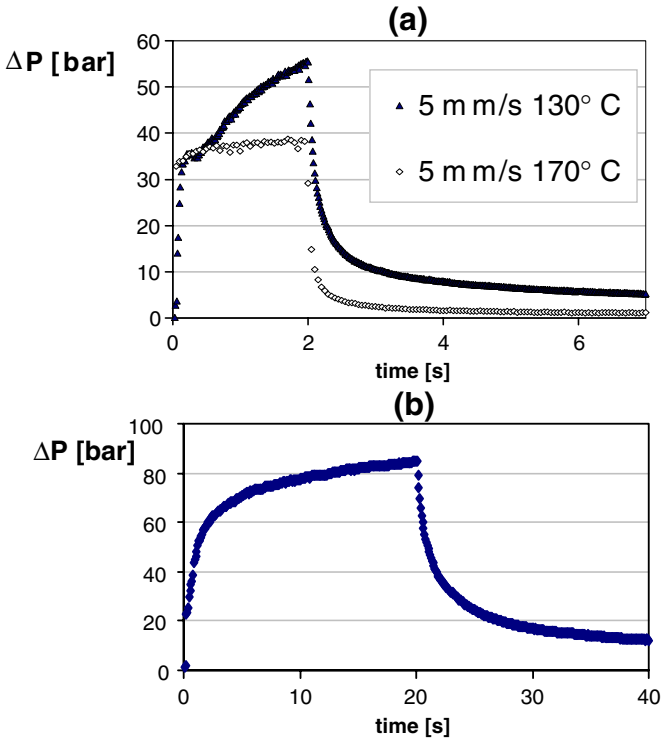

Fig. 9 Evolution of the pressure drop through the midsection as a function of time. **a** HDPE in the deep slit, T=130 and 170 °C, V_P=5 mm/s ($\dot{\gamma}_{app,w}\approx 200\ s^{-1}$) and amplitude=10 mm. t=0, pistons start moving; t=2 s, pistons stop. Note the continuous build up in ΔP during flow associated with FIC when T=130°C as opposed to the melt flow case at 170°C in which the pressure drop reaches a steady-state value. **b** Analogous pressure drop build up in a shallow slit due to flow-induced crystallisation of HDPE. V_P=0.5 mm/s, amplitude=10 mm and T=130°C

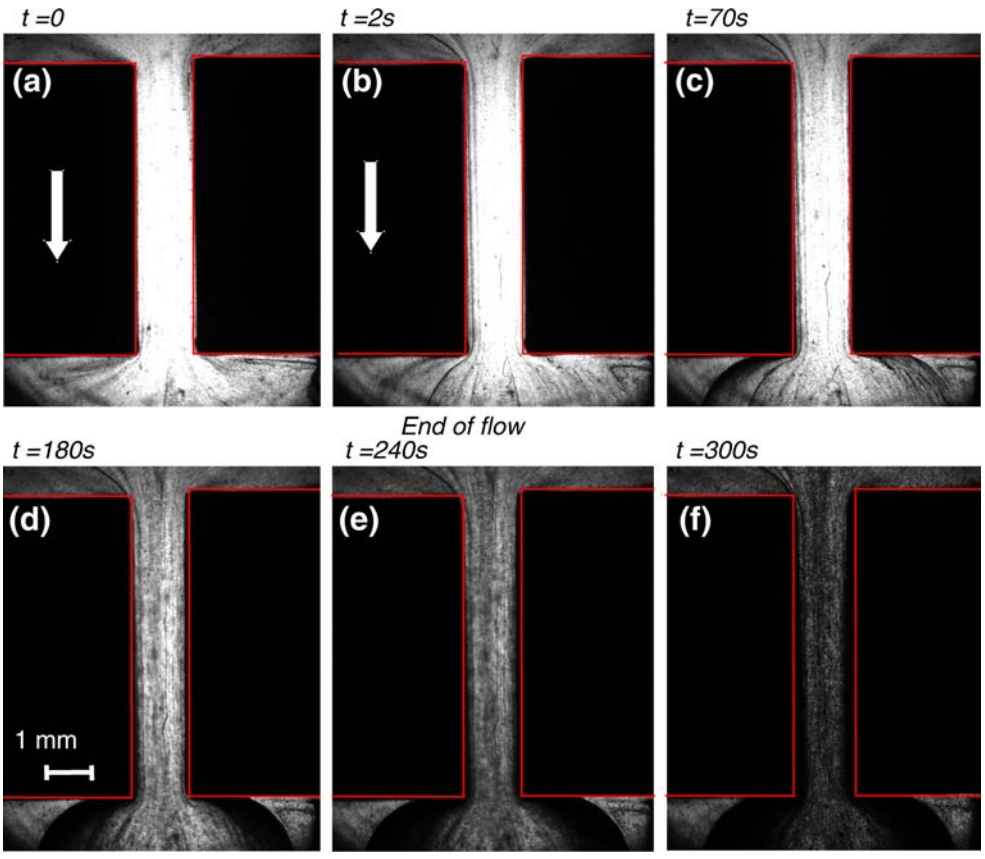

Fig. 10 FIC of PP in the deep slit; T=134 °C; 5 mm/s piston speed, $\dot{\gamma}_{app,w}\approx 200\ s^{-1}$ (We=200). Optical observation in bright field. **a** t=0 (before flow); **b** t=2 s (end of flow). No crystallisation has been detected during flow. **c**–**f** After the flow has stopped, crystallisation evolves preferentially at the fangs region downstream and at the walls, and subsequently everywhere. The morphology cannot be resolved due to the depth of the slit

were carried out at temperatures where no observable spherulitic crystallisation occurred in the absence of flow. Further crystallisation did not develop any further after the flow had stopped, indicating that, under these conditions, flow must be present for fibrous crystals to form. Observations in the deep and shallow slit indicate that flow-induced crystallisation of HDPE originated in both cases from the walls.

Separate in situ wide angle x-ray scattering (WAXS) measurements of HDPE flowing in a 2-mm berillium capillary at an apparent wall shear rate of 28 s^{-1} and 130 °C showed the presence of equatorial spots and an amorphous halo (Scelsi 2006), consistent with the findings of Saquet et al. (2000). All the fibrous crystals formed in these experiments are therefore highly oriented at the nanoscale.

PP ATOFINA 3250MR1

In the absence of flow, crystallisation of PP proceeded slowly for temperatures down to approximately 40 °C below the DSC melting temperature (approximately 170 °C). For this reason, PP had a broader operating window for MPR experiments, corresponding to a wider range of observations that could be performed. The experiments presented in this paper were carried out at high degrees of super-cooling (T_C=134–137 °C) to be able to induce crystallisation within timescales that are reasonably short and comparable to those attained for HDPE. Despite the higher degree of super-cooling, PP had a slower crystallisation kinetics than HDPE due to large differences between the two polymers, both in the crystal nucleation density and in the growth rate (Eder 1999). In analogy with the observations on HDPE, both slit geometries were used. Also in the case of PP, birefringence images during FIC were not helpful in identifying the stresses due to low birefringence levels.

PP–flow-induced crystallisation–geometry 1 (deep slit)

Figure 10 illustrates the way PP crystallises in a deep slit at 134 °C and an apparent wall shear rate of 200 s^{-1},

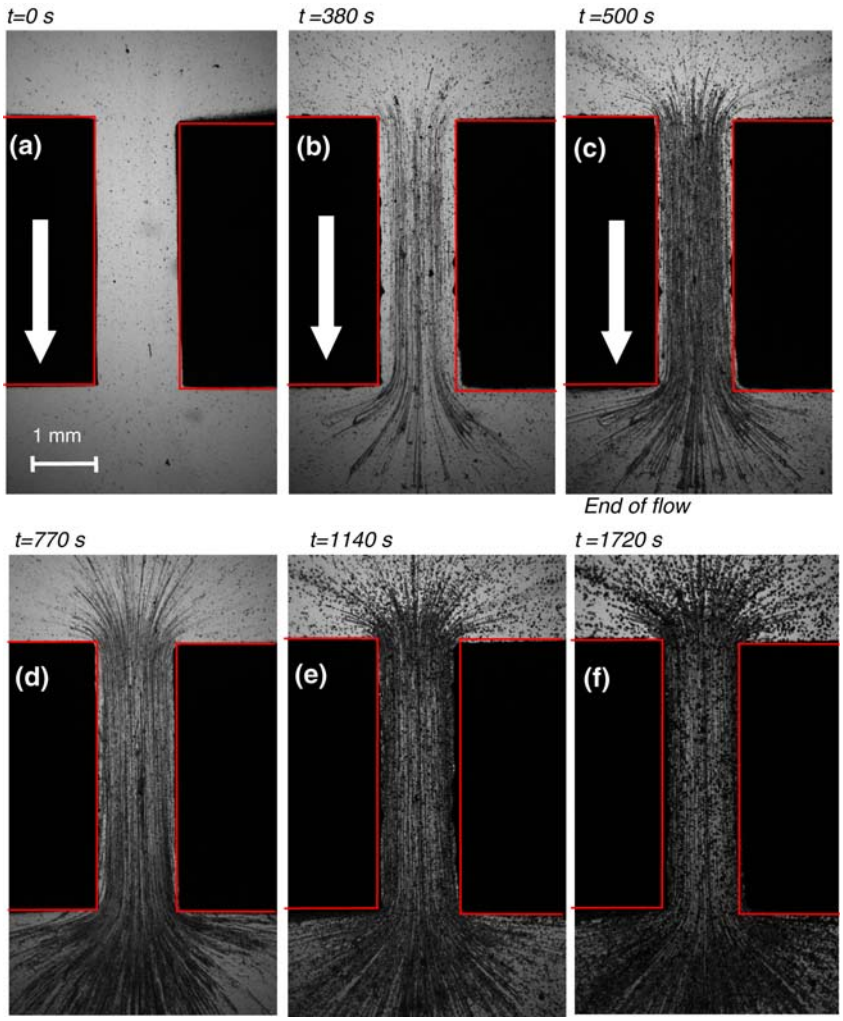

Fig. 11 PP in the shallow slit; T=134°C; 0.02 mm/s piston speed, $\dot{\gamma}_{app,w}\approx 20\ s^{-1}$ (We=20). The fibrous nuclei appear during flow (a–c) and continue to grow after the flow (indicated by the *white arrow*) has stopped, alongside with enhanced spherulitical crystallisation (**d**–**f**)

corresponding to a Weissenberg number of 200. The onset time of quiescent crystallisation in these conditions (36 °C super-cooling) is about 30 min (refer to Fig. 4b). At the start of the experiment, the polymer was uniformly transparent in the entire field of view (Fig. 10a). The pistons were then moved synchronously downwards at 5 mm/s through a displacement of 10 mm. Figure 10b corresponds to the observation just after the pistons had stopped. No visible flow-induced crystals were formed during flow. The matching pressure difference profile is shown in Fig. 13a. The extrusion pressure difference during flow reached a constant steady-state value, did not change during the piston movement and then quickly relaxed to zero after flow cessation. Visible FIC developed with subsequent time after the flow had stopped. Within 70 s, flow-induced crystallisation was visible at the wall of the slit inserts and in the fang regions (Fig. 10c). Crystallisation then evolved preferentially in those regions and also in the rest of the field of view, gradually propagating towards the centreline, as shown by the progressive darkening of Fig. 10c–f). After 300 s, the polymer appeared to have crystallised in the entire slit (Fig. 10f). Due to the excessive depth of sample characterising the deep slit, the morphology could not be resolved. It is speculated that the crystals generated were both oriented (shish-kebabs) at the slit walls and at the fang regions, and unoriented (enhanced spherulites) in the rest of the field of view. The oriented crystals developed with a faster kinetics. In this case, flow enhanced nucleation and growth kinetics of both oriented and unoriented crystallisation.

The optical observations of both HDPE and PP crystallising from the side walls in a deep slit are consistent with those of McHugh et al. (1991) and Saquet et al. (2000).

PP–flow-induced crystallisation–geometry 2 (shallow slit)

A higher resolution of the morphology of the crystallising polymer was achieved by using a shallow slit geometry (1 mm-deep). However, the flow was in this case fully 3D, and the walls of the glass windows had a significant influence on both the flowfield and FIC development.

Figure 11 illustrates a single-pass experiment carried out at 134 °C and a piston speed of 0.02 mm/s, corresponding to an apparent wall shear rate of 20 s^{-1} and Weissenberg number of 20. The flow direction was downwards, as indicated by the arrows. The corresponding pressure difference profile can be found in Fig. 13b.

Several spherulites were already present before the application of flow. Figure 11a shows that these were evenly distributed in the entire view field and were barely visible due to their small starting size. These crystallites have an influence on the subsequent flow-induced crystallisation because they both affect the flow field and act as

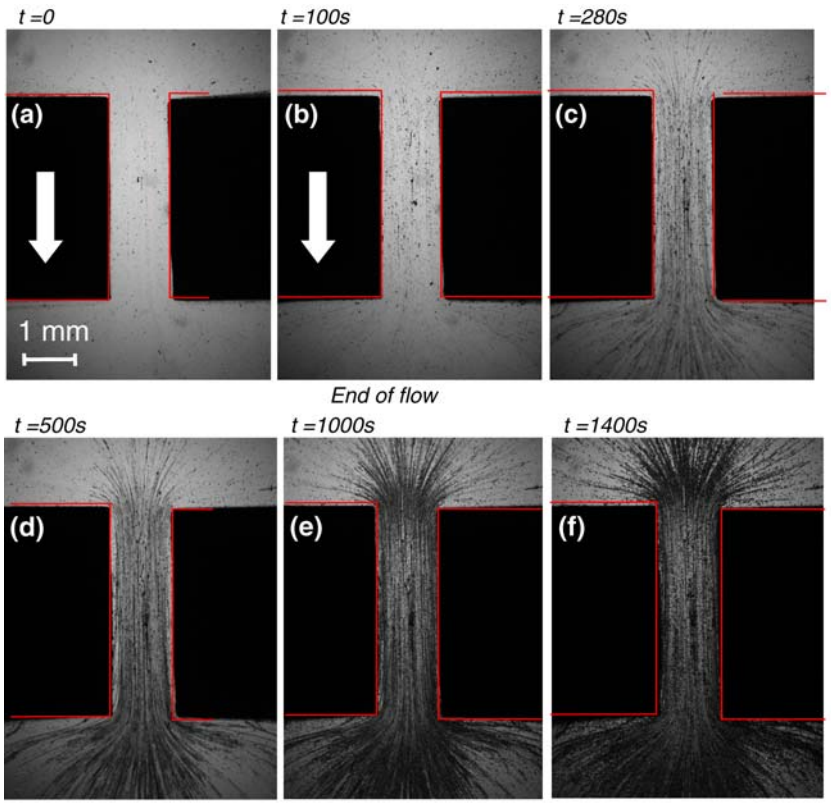

Fig. 12 PP in the shallow slit; T=137 °C; 0.1 mm/s piston speed, $\dot{\gamma}_{app,w} \approx 100\ s^{-1}$ (We=100). The fibrous nuclei are generated during the flow (**a**, **b**), but in this case, they become visible after flow (**c**) and continue to grow throughout the observation time, alongside with enhanced spherulitical crystallisation (**d**–**f**)

physical cross-links, increasing the effective relaxation time of the material. To fully understand the observations, it will then be necessary to estimate the nucleation and growth kinetics of the spherulitic crystallisation that occurs during cooling.

Then, the pistons were moved at a very low speed for a total time of 500 s. Figure 11b was captured during flow and illustrates the progressive appearance of lines in the slit region. These elongated lines were parallel to the streamlines and slowly built up, both in number and lateral diameter over the flow time. At flow cessation (Fig. 11c), they occupied the entire slit region. The streaks formed at the glass walls and were not advected downstream by the flow. It is possible that these lines were generated as a result of the relative motion between the main flow and small spherulites anchored to the glass wall. Simultaneously, spherulitic growth continued to develop at an enhanced rate throughout the observation time. Figure 13b shows the matching extrusion pressure difference profile for this experiment. As in all the other experiments on PP presented in this paper, the pressure difference during flow reached an approximately constant value, showing that crystallisation did not have a significant effect on the flow. The optical observations continued for approximately 25 min after the flow cessation. Figure 11d–f illustrates the development of FIC during that time. No further streaks were generated, but those already present appeared to thicken. It is thought that the lateral growth of the fibrous line crystals corresponded to chain-folded lamellar growth around the line nuclei. The fibrous line crystals also appeared to grow longitudinally both at the entry and at the exit regions (Fig. 11c–f). It is thought that the longitudinal growth was just apparent due to the thickening of the parts of the line crystals that were not previously visible. Enhanced spherulitic growth also proceeded, and some spherulites appeared positioned on the streaks. After 25 min, crystallisation was complete in the slit region and downstream (Fig. 11f).

In the case of PP, the nucleation induced by flow and the subsequent crystal growth were decoupled, and thus, the modeling of the phenomenon is expected to be consider-

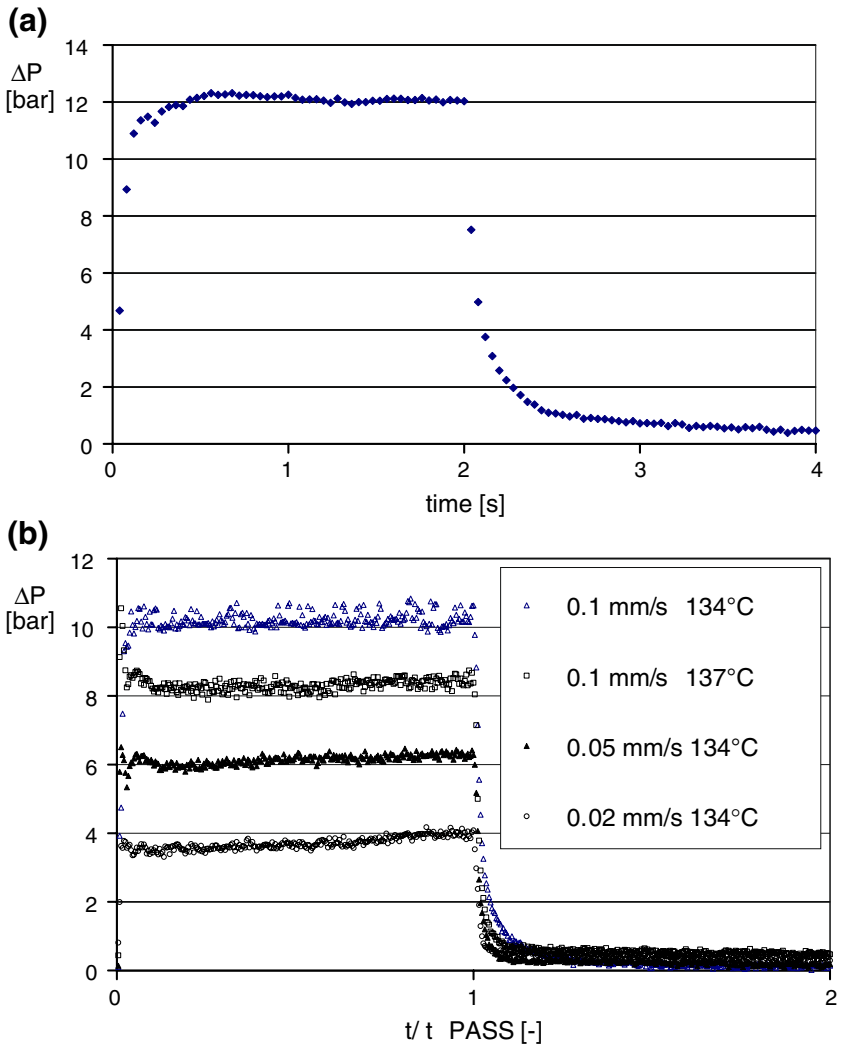

Fig. 13 Evolution of the pressure drop through the midsection as a function of time. **a** PP in the deep slit; T=134 °C; V_P=5 mm/s ($\dot{\gamma}_{app,w}$≈200 s^{-1}); amplitude=10 mm. t=0, pistons start moving; t=2 s, pistons stop. The pressure drop reaches a constant, steady-state value and then relaxes back to zero after the flow has ceased. **b** Analogous pressure drop profiles (no substantial pressure build up during flow) in a shallow slit during flow-induced crystallisation of PP at low deformation rates and similar super-cooling. V_P=0.02–0.1 mm/s, amplitude=10 mm and T=134–137 °C. Time normalised to the time of flow

ably simplified. However, the additional effect of quiescent nucleation before shearing has a relevant influence on the way FIC of PP develops during the experiments and must be included to accurately model the results. Oriented precursors formed throughout the width of the channel in Figs. 10 and 11, in which point-like precursors already existed throughout the melt before inception of flow, but not in Figs. 7 and 8, in which negligible nucleation occurred, except where it was induced by flow.

A similar experiment is shown in Fig. 12. In this case, the temperature, the apparent wall shear rate and Weissenberg number were slightly higher (respectively 137 °C, 100 s^{-1} and We=100). Under these conditions, the elongated crystals generated by the flow were not visible at flow cessation (Fig. 12b). Only after several minutes did these structures appear due to lateral growth. The subsequent FIC development and the pressure difference profile (Fig. 13b) did not differ qualitatively from those in the previous experiment.

Figures 11 and 12 show that the fibre-like structures also appeared in the entry region of the slit. This is due to another abrupt contraction further upstream that occurs at the point in which the flowing polymer encounters the walls of the quartz windows and is squeezed between them.

In situ WAXS measurements of PP flowing in a 2-mm berillium capillary at an apparent wall shear rate of 28 s^{-1} and 132 °C showed an arcing in the diffraction rings, revealing that not only spherulites are present but also oriented lamellae (Scelsi 2006). It was therefore speculated that the oriented crystal structures visible in the experiments on PP discussed in this paper were shish-kebabs rather than regions of bulk crystal comprised of spherulitic material.

Conclusions

MPR experiments were performed to examine the FIC behaviour of HDPE and PP under isothermal conditions at levels of super-cooling and shear rates similar to those encountered in industrial forming processes. Under these conditions, flow-induced crystallisation of HDPE and PP generally occurs in different ways. Crystallisation of HDPE at low super-cooling occurs during flow, and observation reported in this paper is consistent with the observation of Saquet et al. (2000). If crystallisation occurs during flow, the presence of the crystals itself will influence the local growth conditions in a way discussed by Mackley (1975) for HDPE solution growth and Mackley et al. (1975) for melt crystal growth. Observations of both deep and shallow slit geometries support the conclusion that nucleation initiates from the region of the wall. Crystallisation evolves in the fang region of the flow, and the extrusion pressure is influenced by the presence of the HDPE crystals.

In contrast, it was found that visible flow-induced crystallisation of PP occurred predominantly after flow cessation. Again, the walls appeared to produce preferential nucleation sites. Again, preferential flow-induced crystallisation occurred in the region near the walls. FIC developed after flow cessation, and the extrusion pressure did not change during the experiments. The effect of flow was to both induce FIC nucleation and enhance subspherulitic crystal growth. It can be concluded that, during flow, submicron flow-induced fibrous crystal nuclei are formed and that subsequent crystal growth occurs from these nuclei after flow cessation. From the experiments described in this paper, it is probable that modelling flow-induced crystallisation of PP will be easier than modelling FIC of HDPE because, in the case of PP, the flow-induced nucleation can be decoupled from quiescent growth.

At the levels of super-cooling selected in this paper, no or little spherulitic crystallisation was optically or rheologically detectable at the start of flow. This however does not mean that the nucleation process had not begun. It is possible, indeed probable, that nanoscale crystal nuclei had formed before the onset of flow, and it is primarily the subsequent flow behaviour of these nuclei in the flow that results in FIC rather than just the flow behaviour of individual chains.

Acknowledgement We would like to acknowledge D. G. Hassell, G. Hernandez de Muller and S. A. Butler for useful help and advice. We also acknowledge the EPSRC for funding through the μPP^2 program (Microscale Polymer Processing 2). Our final thanks to Dow Benelux and Atofina for providing the materials.

References

Avrami M (1939) Kinetics of phase change. J Chem Phys 7:1103–1112

Billon N, Henaff V, Pelous E, Haudin JM (2002) Transcrystallinity effects in high-density polyethylene. I. Experimental observations in differential scanning calorimetry analysis. J Appl Polym Sci 86(3):725–733

Brochard F, De Gennes PG (1992) Shear-dependent slippage at a polymer/solid interface. Langmuir 8:3033–3037

Clemeur N, Rutgers RPG, Debbaut B (2004) Numerical evaluation of three dimensional effects in planar flow birefringence. J Non-Newton Fluid Mech 123(2-3):105–120

Collis MW, Mackley MR (2005) The melt processing of monodisperse and polydisperse polystyrene melts within a slit entry and exit flow. J Non-Newton Fluid Mech 128(1):29–41

Doufas AK, Dairanieh IS, McHugh AJ (1999) A continuum model for flow-induced crystallization of polymer melts. J Rheol 43(1):85–109

Eder G, Janeschitz-Kriegl H, Liedauer S (1990) Crystallization processes in quiescent and moving polymer melts under heat transfer conditions. Prog Polym Sci 15(4):629–714

Eder G (1999) Crystallization in polymer processing: modelling and experimentation. In: Arkeryd L, Bergh J, Brenner P, Pettersson L

(eds) Progress in industrial mathematics at ECMI 98. Teubner, Leipzig, pp 138–145

Hassell DG, Mackley MR (2008) Localised flow induced crystallisation of a polyethylene melt. Rheol Acta (in press). DOI 10.1007/s00397-008-0263-6

Hernandez de Muller G (2007) The effect of flow on the crystallisation of Polyethylene. PhD thesis, University of Cambridge

Jay F, Haudin JM, Monasse B (1999) Shear-induced crystallization of polypropylenes: effect of molecular weight. J Mater Sci 34 (9):2089–2102

Jerschow P, Janeschitz-Kriegl H (1996) On the development of oblong particles as precursors for polymer crystallization from shear flow: origin of the so-called fine grained layers. Rheol Acta 35 (2):127–133

Keller A (1968) Polymer crystals. Rep Prog Phys 31:623–704

Keller A, Mackley MR (1974) Chain orientation and crystallization. Pure Appl Chem 39:193

Kornfield JA, Kumaraswamy G, Issaian AM (2003) Recent advances in understanding flow effects on polymer crystallization. Ind Eng Chem Res 41:6383–6392

Lee K, Mackley MR, Mcleish TCB, Nicholson TM, Harlen O (2001) Experimental observation and numerical simulation of transient ''stress fangs'' within flowing molten polyethylene. J Rheol 45 (6):1261–1277

Mackley MR (1975) Shish Kebabs: hydrodynamic factors affecting their crystal growth. Colloid and Polym Sci 253:373–379

Mackley MR, Frank FC, Keller A (1975) Flow induced crystallization of polyethylene melts. J Mater Sci 10:1501–1509

Mackley MR, Marshall RTJ, Smeulders JBAF, Zhao FD (1994) The rheological characterization of polymeric and colloidal fluids. Chem Eng Sci 49:2551–2565

McHugh AJ, Khomami B (1990) Flow history—morphology development in crystallizable polymer melts. Int Polym Process V:252–257

McHugh AJ, Tree DA, Pornimit B, Ehrenstein GW (1991) Flow-induced crystallization and self-reinforcement during extrusion. Int Polym Process VI:208–211

Peters GMW (2003) A computational model for processing of semi-crystalline polymers: the effects of flow-induced crystallization. Lect Notes Phys 606:312–324

Saquet O, Mackley MR, Moggridge G (2000) Direct experimental evidence for flow induced fibrous polymer crystallisation occurring at a solid/melt interface. J Mater Sci 35:5247–5253

Scelsi L (2006) Flow-induced crystallisation of polyethylene and polypropylene melts. Certificate of Postgraduate Study, Department of Chemical Engineering, University of Cambridge

Smirnova J, Silva L, Monasse B, Chenot J, Haudin J (2005) Structure development in injection molding. Int Polym Process 20(2):178–185

Somani RH, Hsiao BS, Nogales, A, Srinivas S, Tsou AH, Sics I, Balta-Calleja FJ, Ezquerra TA (2000) Structure development during shear flow-induced crystallization of i-PP: In Situ Small-Angle X-ray Scattering Study. Macromolecules 33:9385–9394

Swartjes FHM (2003) Stress induced crystallization in elongational flow. PhD thesis, TU Eindhoven

Valette R, Mackley MR, Hernandez G (2006) The comparison of experimental time-dependent birefringence and pressure data with a compressible flow, Rolie Poly viscoelastic numerical simulation. J Non-Newton Fluid Mech 136:118–125

Van Meerveld J, Peters GWM, Hütter M (2004) Towards a rheological classification of flow induced crystallization experiments of polymer melts. Rheol Acta 44:119–134

Zuidema H, Peters GWM, Meijer HEH (2001) Development and validation of a recoverable strain-based model for flow-induced crystallization of polymers. Macromol Theory Simul 10:447–460